A novel nanobody that detects the gain-of-function phenotype of von Willebrand factor in ADAMTS13 deficiency and von Willebrand disease type 2B

Janine J. J. Hulstein, Philip G. de Groot, Karen Silence, Agnès Veyradier, Rob Fijnheer, and Peter J. Lenting

Von Willebrand factor (VWF) is unable to interact spontaneously with platelets because this interaction requires a conversion of the VWF A1 domain into a glycoprotein Ibα (GpIbα) binding conformation. Here, we discuss a llama-derived antibody fragment (AU/VWFa-11) that specifically recognizes the GpIbα-binding conformation. AU/VWFa-11 is unable to bind VWF in solution, but efficiently interacts with ristocetin- or botrocetin-activated VWF, VWF comprising type 2B mutation R1306Q, or immobilized VWF. These unique properties allowed us to use AU/VWFa-11 for the detection of activated VWF in plasma of patients characterized by spontaneous VWF-platelet interactions: von Willebrand disease (VWD) type 2B and thrombotic thrombocytopenic purpura (TTP). For VWD type 2B, levels of activated VWF were increased 12-fold (*P* < .001) compared to levels in healthy volunteers. An inverse correlation between activated VWF levels and platelet count was observed (R^2 = 0.74; *P* < .003). With regard to TTP, a 2-fold (*P* < .001) increase in activated VWF levels was found in plasma of patients with acquired TTP, whereas an 8-fold increase (*P* < .003) was found in congenital TTP. No overlap in levels of activated VWF could be detected between acquired and congenital TTP, suggesting that AU/VWFa-11 could be used to distinguish between both disorders. Furthermore, it could provide a tool to investigate the role of VWF in the development of thrombocytopenia in various diseases. (Blood. 2005;106: 3035-3042)

Introduction

Adhesion of platelets to the injured vessel wall is a multistep process, involving several components, including von Willebrand factor (VWF). VWF is an adhesive glycoprotein that circulates in plasma as an array of multimeric subunits.[1] This multimeric structure allows VWF to function as a molecular bridge between the subendothelial matrix and the platelet surface glycoprotein (Gp) Ib/IX/V receptor complex. Complex formation between VWF and the GpIb/IX/V receptor is of particular importance for the tethering of platelets on vascular surfaces exposed to rapidly flowing blood.[2]

The interaction between VWF and the GpIb/IX/V complex is mediated by specific regions of both components; VWF residues 1238-1481 (the so-called A1 domain) comprise an interactive site for residues 1-290 of GpIbα.[3] Although the structure of this complex has been solved at the atomic level,[4] some issues regarding this interaction have remained unclear. For instance, despite the notion that VWF and GpIbα coexist in the circulation, their interaction does not occur under normal conditions. In contrast, the isolated recombinant A1 domain does display spontaneous binding to GpIbα. Apparently, a shift from a nonbinding to a binding mode of the VWF A1 domain in its multimeric environment is required to induce complex formation.[4] However, the molecular basis of this activation step is largely unknown.

Activation of the A1 domain can be induced by several means. Nonphysiologic activation of the A1 domain occurs through direct immobilization of purified VWF onto artificial surfaces, such as glass or plastic. In vitro activation of VWF is also achieved by the addition of modulators, such as the snake venom component botrocetin or the antibiotic ristocetin.[5,6] Furthermore, physiologic activation of VWF is induced on its binding to the subendothelial matrix component collagen or under conditions of very high shear stress.[7] Also, various pathologic conditions may lead to premature complex formation between VWF and platelet GpIbα. Some gain-of-function mutations in the VWF A1 domain may increase the affinity for GpIbα. Such mutations are associated with von Willebrand disease (VWD) type 2B; these patients are characterized by loss of high-molecular-weight multimers from plasma, increased ristocetin-induced platelet aggregation, a prolonged bleeding time, and thrombocytopenia.[8,9] Another condition that has been reported to allow spontaneous platelet adhesion relates to the size of multimeric VWF. Multimeric VWF is stored in Weibel-Palade bodies in endothelial cells and released on stimulation.[10-12] The newly released VWF is enriched in ultralarge (UL)–VWF multimers, which have the potential to bind platelets in the absence of any modulators or high shear stress.[13] Direct release of the UL-VWF molecules in the circulation is prevented by proteolysis of these multimers at the endothelial surface.[14] This process is

From the Laboratory for Thrombosis and Haemostasis, Department of Haematology, University Medical Center Utrecht, Utrecht, The Netherlands; Ablynx, Ghent, Belgium; INSERM U143Le Kremlin-Bicêtre, France; and Jeroen Bosch Hospital, Location Groot Ziekengasthuis, Department of Internal Medicine, Den Bosch, The Netherlands.

Submitted March 22, 2005; accepted June 24, 2005. Prepublished online as *Blood* First Edition Paper, July 12, 2005; DOI 10.1182/blood-2005-03-1153.

Supported by a grant of the Landsteiner Foundation of Blood Transfusion Research (LSBR grant no. 01.14) and the Noaber Foundation.

K.S. has declared a financial interest in Ablynx, whose nanobody was studied in the present work. K.S. is employed by Ablynx, whose nanobody was studied in the present work.

Reprints: Peter J. Lenting, Laboratory for Thrombosis and Haemostasis, Department of Haematology, G03.647, University Medical Center Utrecht, PO Box 85500, 3584 CX Utrecht, The Netherlands; e-mail: p.j.lenting@azu.nl.

The publication costs of this article were defrayed in part by page charge payment. Therefore, and solely to indicate this fact, this article is hereby marked "advertisement" in accordance with 18 U.S.C. section 1734.

mediated by the recently identified protease ADAMTS13, which cleaves mature VWF between residues M1605 and Y1606.[15,16] Once cleaved by ADAMTS13, the residual multimers have lost the ability to bind platelets spontaneously. The importance of ADAMTS13 activity is illustrated by the life-threatening disease thrombotic thrombocytopenic purpura (TTP), in which ADAMTS13 activity is low or absent. ADAMTS13 deficiency is caused by inhibiting antibodies (acquired TTP)[17] or by mutations in the gene encoding ADAMTS13 (congenital TTP).[18,19] In the absence of ADAMTS13 activity, an excess of UL-VWF multimers is released into the circulation, which leads to spontaneous platelet binding and subsequent thrombus formation in the microvasculature.[20] This causes hemolytic anemia, renal failure, neurologic deficits, fever, and, if not treated well, coma and death.[21]

Although VWD type 2B and TTP are associated with different phenotypic appearances, they have in common that at least part of the circulating VWF multimers should exist in an active conformation. The presence of activated VWF can be determined indirectly by measuring ristocetin-dependent platelet aggregation. However, this method is rather insensitive and is difficult to use when VWF antigen levels are low. In the present paper, we describe a recombinant llama-derived antibody fragment that recognizes immobilized VWF but not VWF in solution, suggesting that this antibody fragment recognizes an epitope within the VWF A1 domain that becomes exposed on activation of VWF. This antibody fragment was subsequently used to monitor the presence of activated VWF in plasma samples from patients with VWD type 2B and TTP. The analysis revealed that in the circulation of both patient groups the levels of activated VWF are elevated 2- to 12-fold compared to levels in healthy individuals.

Patients, materials, and methods

Proteins and antibodies

Recombinant GpIbα (residues 1-290) was expressed and purified as described.[4] Botrocetin was purchased from Kordia Laboratory Supplies (Leiden, The Netherlands). Plasma-derived (pd) VWF was purified from cryoprecipitate (Haemate P 250 IE, Behringwerke, Marburg, Germany) as described.[22] Bovine serum albumin (BSA) and human placental collagen type III were from Sigma (St Louis, MO) and human albumin (fraction V) was from MP Biochemicals (Irvine, CA). Polyclonal antibodies against VWF and horseradish peroxidase (HRP)–conjugated antibodies against VWF and HRP-conjugated rabbit anti–mouse antibody were obtained from DakoCytomation (Glostrup, Denmark).

Construction and expression of recombinant proteins

Construction of expression vector pNUT encoding wild-type (wt) VWF and VWF with VWD type 2B mutation R1306Q was described previously.[23,24] VWF/A1(1261-1468) and VWF/A1(1261-1468)-R1306Q were cloned into expression vector pPIC9 and overexpressed in Pichia Pastoris.[4] pNUT-VWF/A1(1238-1481) was constructed by generating a polymerase chain reaction (PCR) product with forward primer 5′-GGATCCCAGGAGCCGGGAGGCCTGG TGG-3′ and reverse primer 5′-GCGGCCGCCCCCGGGCCCACAGTGACTTG-3′, for which pNUT-VWF served as template. After sequence analysis, the *Bam*HI-*Not*I fragment was ligated into a *Bam*HI-*Not*I–digested pNUT vector containing a C-terminal 6-histidine tag. Wt VWF, VWF/R1306Q, and VWF/A1(1238-1481) were stably expressed in baby hamster kidney cells, which also overexpress furin for proper removal of the propeptide.[23] The full-length proteins were purified from conditioned serum-free medium as described.[25] VWF/A1(1238-1481) was purified from expression medium using Ni^{2+}/NTA chromatography.[4] VWF/A1(1261-1468) and VWF/A1(1261-1468)-R1306Q were purified on heparin-Sepharose, followed by gel filtration.[4] Analysis on sodium dodecyl sulfate (SDS)–polyacrylamide gel electrophoresis showed that all recombinant proteins were purified to homogeneity. The multimeric structure of wt VWF and VWF/R1306Q was analyzed using 0.1% SDS, 1% agarose gel electrophoresis as described previously.[26]

Production and selection of recombinant llama antibody fragments (nanobodies) via phage-display technology

Llama antibodies were raised by immunization with a wt VWF preparation containing high-molecular-weight multimers using standard immunization protocols. Total RNA was isolated from peripheral blood lymphocytes and used as a template for the preparation of cDNA to amplify the repertoire of variable domains of the antibody heavy chains.[27] This repertoire was then subcloned to allow selection of nanobodies via phage display.[27] For the selection of the nanobodies, the wells of a maxisorp-microtiter plate (Nunc, Roskilde, Denmark) were coated with 5 μg/mL VWF/A1(1238-1481) in 50 mM $NaHCO_3$ (pH 9.6, overnight at 4°C). After washing and blocking (phosphate-buffered saline [PBS]/1% casein), wells were incubated with phages for 2 hours at room temperature. Wells were then washed extensively with PBS, and bound phages were eluted with 0.2 M glycine (pH 2.4, 20 minutes at room temperature). The eluted phages were added to exponentially growing *Escherichia coli* TG1 cells, which were then plated onto Luria broth (LB)–ampicillin. In the second round of selection, phages were resuspended in the presence of 10 μg/mL wt VWF before incubation in wells coated with VWF/A1(1238-1481) wells. This selection strategy was chosen to isolate nanobodies that specifically recognize A1 domain in its GpIbα-binding conformation and not A1 domain in its resting conformation. After washing the wells 7 times for 30 minutes in the presence of 10 μg/mL wt VWF, bound phages were eluted and used for transduction of TG1 cells to isolate single clones after plating on LB-ampicillin. Subsequently, single colonies were picked for reinfection of TG1 cells and expression of phage gen3-nanobody fusion proteins was induced on the addition of 1 mM isopropyl-1-thio-β-D-galactopyranoside. Periplasmic proteins were extracted as described[28] and analyzed for binding to immobilized VWF/A1(1238-1481). DNA of positive clones was then analyzed via *Hin*fI digestion and those with appropriate inserts were used for transformation to the nonsuppressor *E coli* WK-6 strain,[27] which allows the expression of nanobodies in the absence of the phage gen3-protein. Periplasmic samples were prepared as described[27] and nanobodies were purified to homogeneity using $Ni2^{+}$/NTA resin. The control nanobody used in the present study was obtained after immunization with and selection using the isolated recombinant VWF A1 domain.

Competition assay

The specificity of the interaction between AU/VWFa-11 and activated VWF was assessed in an immunosorbent assay, in which purified pd-VWF (3.7 nM, based on monomeric structure) was immobilized in microtiter wells (Costar, Cambridge, MA). Wells were blocked with PBS containing 3% BSA and 0.1% Tween-20 for 1 hour at 37°C and incubated with different concentrations of biotinylated control nanobody and AU/VWFa-11 (0-625 nM) in PBS for 1 hour at 37°C. Binding of the nanobodies was monitored with HRP-conjugated streptavidin and the nanobody concentration at half maximum binding was determined. These concentrations were used in the competition assay, in which pd VWF-coated wells were incubated with either of the nanobodies in the presence or absence of the indicated concentrations of wt VWF or wt VWF preincubated with 1 mg/mL ristocetin (5 minutes at room temperature; 0-115 nM soluble VWF for the control nanobody and 0-38 nM for AU/VWFa-11) or in the presence of a 10-fold molar excess of VWF/R1306Q or VWF/A1(1261-1468)-R1306Q. After washing, wells were incubated with HRP-conjugated streptavidin (DakoCytomation) and binding was detected by measuring HRP activity using *o*-phenylenediamine (OPD) as substrate.

Surface plasmon resonance analysis

Surface plasmon resonance (SRP)–binding studies were performed using a Biacore 2000 system (Biacore, Uppsala, Sweden). AU/VWFa-11 was immobilized on a CM5 sensor chip using the amine-coupling kit as instructed by the supplier (Biacore). V128H, a nanobody recognizing the A3 domain of VWF, was used as a control. Binding of VWF/A1(1238-1481), VWF/A1(1261-1468), and VWF/A1(1261-1468)-R1306Q to the AU/VWFa-11–coated channel was corrected for binding to the V128H-coated channel. Binding of VWF constructs to the immobilized nanobodies was performed in 150 mM NaCl, 25 nM HEPES (N-2-hydroxyethylpiperazine-N′-2-ethanesulfonic acid), 0.005% Tween-20 (pH 7.4) at 25°C with a flow rate of 20 μL/min. Regeneration of the surface was performed by subsequent application of 50 mM triethyl amine and formate buffer (10 mM $NaHCO_2$ and 150 mM NaCl, pH 2.0).

Binding of AU/VWFa-11 and GpIbα to VWF/R1306Q in immunosorbent assay

Microtiter wells (Costar) were coated overnight at 4°C with 5 μg/mL AU/VWFa-11 and blocked with PBS/3% BSA/0.1% Tween-20 (30 minutes at 37°C). After washing with PBS/0.1% Tween-20, wells were incubated with 3.7 nM VWF/R1306Q (1 hour at 37°C). Wells were washed and incubated 1 hour at 37°C with GpIbα (0.12-31.1 nM). After washing 3 times, wells were incubated with a monoclonal anti-GpIbα antibody and binding was detected with an HRP-conjugated rabbit anti–mouse antibody.

Static adhesion of CHO cells expressing the GpIb/IX/V complex to immobilized VWF

Wt VWF (37 nM) was immobilized overnight at 4°C in microtiter wells (Nunclon; Nunc) in 50 mM $NaHCO_3$ (pH 9.6). Wells were blocked with 0.5% polyvinylpyrrolidone in PBS for 1 hour at room temperature and incubated with 1.25 μM AU/VWFa-11 or control nanobody (1 hour at room temperature). After washing 3 times with PBS, CHO cells expressing the GpIb/IX/V complex (generous gift of Dr J. A. Lopez,[29] 1×10^5 cells in Dulbecco modified Eagle medium [DMEM] containing 0.1% BSA) were allowed to bind to immobilized VWF (90 minutes at 37°C) in the presence or absence of control nanobody or AU/VWFa-11 (1.25 μM). Wells were washed and binding of cells was detected by measuring the intrinsic alkaline phosphatase activity of the CHO cells, using *p*-nitrophenol phosphate (PNP; Sigma) as a substrate diluted in lysis buffer (3 mg/mL PNP in 1% Triton X-100, 50 mM acetic acid, pH 5.0).

Platelet adhesion to collagen type III and VWF

Perfusions over collagen type III were carried out with whole blood, drawn from healthy volunteers who denied ingestion of aspirin or other nonsteroidal anti-inflammatory drugs for the preceding 10 days, into 0.1 volume of 50 μg/mL PPACK (H-D-Phe-Pro-Arg-chloromethylketone; Bachem, Torrence, CA) and 20 U/mL pentasaccharide. Thermanox coverslips (Nunc) were coated with collagen type III[30] and whole blood was perfused over the coverslips for 5 minutes at 1600 s^{-1}. Perfusions over VWF-coated coverslips were performed with reconstituted blood. To obtain reconstituted blood, platelets were mixed with red blood cells to a platelet count of 200 000 platelets/μL and a hematocrit of 40%.[30] Perfusion was performed at a shear rate of 1600 s^{-1}. After perfusion, slides were washed, fixed, and stained[30] and platelet adhesion was evaluated using computer-assisted analysis with OPTIMAS 6.0 software (Dutch Vision Systems, Breda, The Netherlands). All perfusions were performed 3 times.

Patient materials

Plasma samples from healthy donors (n = 9), patients with VWD type 2B (n = 10), and patients with acquired (n = 12) or congenital TTP (n = 5) were collected in 3.1% citrate using a Vacutainer system. VWD type 2B was diagnosed in families with the typical pattern of an autosomal inherited bleeding disorder with thrombocytopenia, low ristocetin-induced platelet aggregation, and the absence of high multimeric VWF multimers on gel electrophoresis. The mutations in VWF of these patients have not been determined. Patients with acquired TTP were characterized by thrombocytopenia, Coombs-negative hemolytic anemia, and the presence of fragmented erythrocytes in peripheral blood. Other causes for hemolytic anemia and thrombocytopenia were excluded and all patients with TTP were treated with plasma exchange. Response to plasma exchange was observed in all patients. Plasma samples were taken before treatment and ADAMTS13 activity was found to be absent in these samples. Five patients with a congenital form of TTP and a severe deficiency of ADAMTS13 activity were described previously.[31] Platelet-poor plasma was aliquoted and frozen at −80°C. For normal pool plasma (NPP), platelet-poor plasma of 40 healthy donors was pooled and was stored in aliquots at −80°C. All patients gave informed consent for the sampling of blood for scientific purposes. All patients gave informed consent for the sampling of blood for scientific purposes, per the Declaration of Helsinki. Approval was obtained from the institutional review boards of the University Medical Center Utrecht (Utrecht, the Netherlands) and the Robert Debre hospital (Paris, France) for those studies.

Immunosorbent assay for activated VWF

VWF antigen levels were quantified as described before.[26] Microtiter wells (Maxisorb; Nunc) were coated overnight at 4°C with 5 μg/mL AU/VWFa-11 in 50 mM $NaHCO_3$ (pH 9.6) and blocked with PBS/3% BSA/0.1% Tween-20 for 30 minutes at 37°C. Wells were washed 3 times with PBS/0.1% Tween-20 and incubated with culture medium containing wt VWF or VWF-R1306Q in the absence or presence of ristocetin (0.08-1 mg/mL) or botrocetin (0.2 U/mL), or plasma samples (1 hour 37°C). All samples were diluted in PBS to reach a VWF concentration between 0.23 and 1.85 nM. After washing 3 times with PBS/0.1% Tween-20, plates were incubated with HRP-conjugated polyclonal anti-VWF (1.3 μg/mL) in PBS for 1 hour at 37°C. Plates were washed 3 times and binding was detected by measuring the HRP activity using OPD as a substrate (Merck, Darmstadt, Germany). NPP was used as standard in every assay. The ratio between the slope for the different plasma samples over the slope for NPP was designated activation factor. All patient plasmas have been measured in at least 2 individual experiments.

Variation of the AU/VWFa-11 immunosorbent assay

To determine the intraexperiment variation of the AU/VWFa-11 immunosorbent assay, 10 randomly chosen wells of an AU/VWFa-11–coated microtiter plate were incubated with one sample (healthy individual no. 7). Moreover, sample no. 7 was measured in 10 different experiments to determine the interexperiment variation. NPP was used as standard and the activation factor was calculated. The intraexperiment variation was 7.1% and the variation between different experiments was 13.7%.

Data analysis and statistics

Analysis of data obtained from SPR analysis and immunosorbent assays was performed using the GraphPad Prism program (GraphPad Prism version 4.0 for Windows, GraphPad Software, San Diego, CA). All data were expressed as mean with SD. An unpaired *t* test with Welch correction was performed to compare the mean levels of activated VWF between the different patient groups. For comparison of 3 groups, one-way ANOVA was performed followed by Bonferroni correction for the calculation of differences between each group separately. *P* below .05 was considered significant.

Results

Nanobody AU/VWFa-11 specifically recognizes the active conformation of VWF

To obtain antibodies that predominantly recognize activated but not native VWF, a llama was immunized with purified VWF preparations that contained UL-VWF (multimer size exceeding 20 subunits). Subsequently, the antibody repertoire of the animal was cloned, and nanobodies were selected for their ability to bind to immobilized VWF A1 domain in the presence of soluble full-length VWF. Of the nanobodies that were obtained, one was selected for further analysis, AU/VWFa-11. Throughout the study, a nanobody

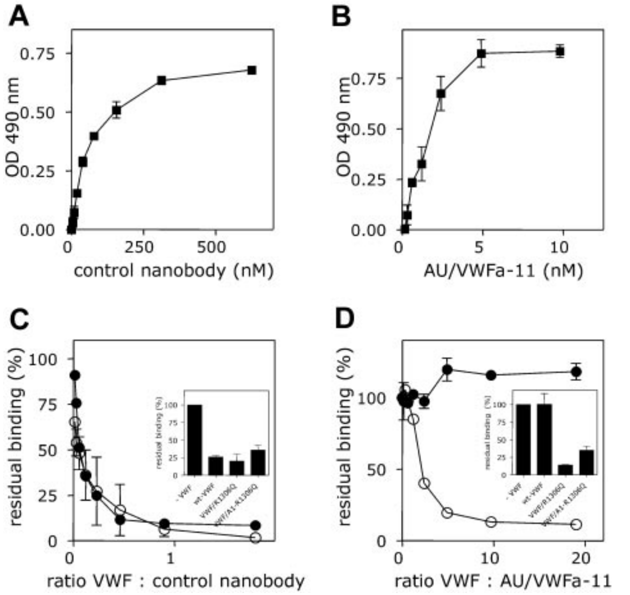

Figure 1. Differential binding of the control nanobody and AU/VWFa-11 to wt VWF and ristocetin-activated VWF. (A-B) Pd VWF was immobilized in microtiter wells (1 μg/mL, overnight at 4°C) and incubated with different concentrations of biotinylated control nanobody (A; 0-625 nM) or AU/VWFa-11 (B; 0-10 nM). Bound nanobody was detected with HRP-conjugated streptavidin. (C-D) Pd VWF-coated microtiter wells were incubated with biotinylated control nanobody (62.5 nM; C) or AU/VWFa-11 (1.9 nM; D) in the absence or presence of different concentrations of wt VWF preincubated with 1 mg/mL ristocetin (5 minutes at room temperature, ○) or wt VWF (●). Concentrations varied from 0 to 90 nM for control nanobody and from 0 to 20 nM for AU/VWFa-11. Inset shows incubation of control nanobody (62.5 nM) or AU/VWFa-11 (1.9 nM) in the presence of a 10-fold molar excess of VWF/R1306Q or VWF/A1(1261-1468)-R1306Q. Bound nanobody was detected using streptavidin-HRP. Binding in the absence of competitors was set to be 100%. Residual binding in the presence of VWF was plotted against the VWF/nanobody ratio. Data represent the mean ± SD of 3 experiments.

obtained after immunization with the isolated A1 domain was used as control nanobody. Nanobody AU/VWFa-11 was examined for its ability to distinguish between native VWF and activated VWF. To this end, purified recombinant wt VWF was immobilized in microtiter wells. This procedure leads to conformational changes in the molecule, allowing the binding of nanobodies that are specific for activated VWF. As expected, both biotinylated nanobodies bound to immobilized VWF in a dose-dependent and saturable manner. Half-maximum binding was obtained at 62.5 nM for the control nanobody or at 1.9 nM for AU/VWFa-11 (Figure 1A-B). These concentrations were used in a competition assay, in which binding of the nanobodies was studied in the presence of different concentrations of soluble wt VWF, wt VWF preincubated with ristocetin, VWF/R1306Q, or VWF/A1(1261-1468). The presence of these competitors considerably reduced binding of biotinylated control nanobody (Figure 1C). Ristocetin-activated VWF, VWF/R1306Q, and VWF/A1(1261-1468)-R1306Q interfered with binding of biotinylated AU/VWFa-11 (Figure 1D). In contrast, binding of AU/VWFa-11 remained unaffected in the presence of a 20-fold molar excess of wt VWF. Apparently, AU/VWFa-11 has the potential to selectively recognize VWF that is, at least in part, in an activated conformation.

Interaction between AU/VWFa-11 and VWF A1 domain

The interaction between nanobody AU/VWFa-11 and the A1 domain of VWF was investigated in more detail. Binding of AU/VWFa-11 to 3 different variants of the A1 domain was compared in a quantitative manner using SPR analysis. VWF/A1(1261-1468), VWF/A1(1238-1481, which comprises longer flanking regions of the A1 domain than VWF/A1(1261-1468), and VWF/A1(1261-1468)-R1306Q (containing the type 2B mutation Arg1306Gln) were perfused over immobilized AU/VWFa-11 (0.06 pmol/mm²) at a flow rate of 20 μL/min until equilibrium was reached. Binding isotherms using the response at equilibrium were used to calculate K_D (Figure 2). This analysis revealed an apparent K_D for VWF/A1(1238-1481) of 1704 nM. Removal of the flanking peptides of the A1 domain resulted in a higher affinity for AU/VWFa-11 (K_D = 81 nM). Moreover, VWF/A1(1261-1468)-R1306Q was bound even more efficiently with an apparent K_D of 44 nM. These results suggest that exposure of the epitope of nanobody AU/VWFa-11 indeed relies on conformational changes within the A1 domain.

GpIbα and AU/VWFa-11 bind different regions within the A1 domain

The conformation induced by ristocetin, immobilization of VWF, or a VWD type 2B mutation promotes binding to GpIbα and this conformation is also specifically recognized by AU/VWFa-11. Therefore, the possibility was considered that AU/VWFa-11 and GpIbα bind to similar regions in the A1 domain. This was first tested in an immunosorbent assay in which binding of GpIbα to nanobody-bound VWF/R1306Q was studied. Immobilization of VWF/R1306Q via the control nanobody interfered with binding of GpIbα. In contrast, GpIbα was able to bind to AU/VWFa-11–bound VWF/R1306Q in a dose-dependent manner (Figure 3A), suggesting that the binding site for AU/VWFa-11 is distinct from the binding site for GpIbα. This was confirmed in a static adhesion assay. Binding of CHO cells expressing the GpIb/IX/V complex to immobilized VWF remained unaffected even in the presence of an excess of AU/VWFa-11 (Figure 3B).

Because the effect of both nanobodies on the binding of VWF to GpIbα may be different under flow conditions, we further examined their effect in a perfusion assay. Human whole blood was perfused over a collagen type III surface at high shear (1600 s^{-1}). Under these conditions, platelet adhesion is fully dependent on the interaction between VWF and GpIbα.[32] In the absence of nanobodies, these conditions resulted in a platelet coverage of 67.8% ± 8.3% (n = 3; Figure 4A). The presence of the control nanobody was associated with a decreased platelet coverage (49.8% ± 4.5% and 24.9% ± 3.1% in the presence of 31.3 and 125 nM nanobody, respectively; Figure 4B). In contrast, even in the presence of 625 nM nanobody AU/VWFa-11, platelet coverage was still similar to

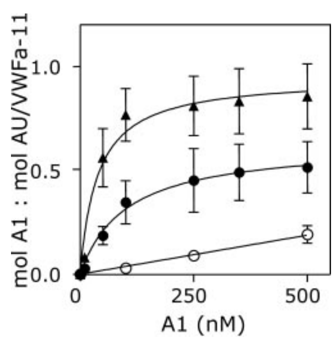

Figure 2. Interaction between AU/VWFa-11 and the VWF A1 domain. Different concentrations of VWF/A1(1238-1481) (○), VWF/A1(1261-1468) (●), or VWF/A1(1261-1468)-R1306Q (▲, 500 nM) were perfused over a CM5-sensor chip coated with 0.06 pmol/mm² AU/VWFa-11 at a flow rate of 20 μL/min. The response at equilibrium (mol A1/mol AU/VWFa-11) was plotted against the concentration of VWF/A1 that was perfused over the chip.

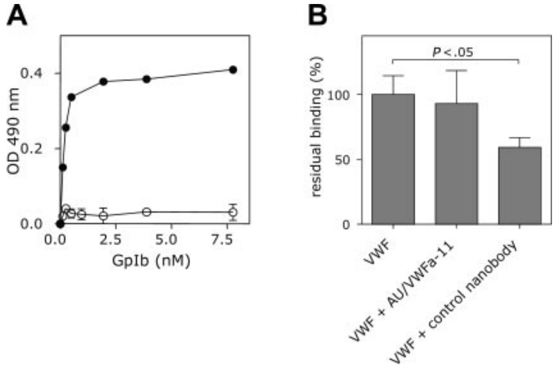

Figure 3. VWF-GpIbα interaction is unaffected by AU/VWFa-11 in static adhesion. (A) Microtiter wells coated with 5 μg/mL AU/VWFa-11 (●) or control nanobody (○) were blocked 30 minutes at 37°C with PBS/3% BSA/0.1% Tween-20 and incubated with 3.7 nM VWF/R1306Q. After washing, wells were incubated with GpIbα (0.12-31.1 nM) and subsequently with a monoclonal anti-GpIb antibody. Wells were washed and incubated with an HRP-conjugated rabbit anti–mouse antibody. Binding was detected by measuring the peroxidase activity. (B) Microtiter wells were coated with wt VWF (37 nM in 50 mM $NaHCO_3$ buffer), overnight at 4°C. After blocking wells 1 hour at room temperature with 0.5% polyvinylpyrrolidone in PBS, wells were incubated with AU/VWFa-11 or control nanobody (1.25 μM in PBS, 1 hour, room temperature). After washing with PBS, CHO cells expressing the GpIb/IX/V complex (1×10^5 cells in DMEM containing 0.1% BSA) were allowed to bind in the presence or absence of the control nanobody or AU/VWFa-11 (1.25 μM). Binding of these cells was monitored by measuring the intrinsic alkaline phosphatase activity of the cells and set to be 100% in the absence of nanobodies. Data represent the mean ± SEM of 3 experiments.

that in its absence (73.3% ± 4.4%; Figure 4C). Moreover, platelet adhesion to a VWF surface remained unaffected in the presence of AU/VWFa-11 (Figure 4D-E). These data are compatible with the view that GpIbα and nanobody AU/VWFa-11 bind to different regions of the A1 domain.

Immunosorbent assay for detection of activated VWF in solution

Although GpIbα and nanobody AU/VWFa-11 bind to distinct sites within VWF, both have in common that they only recognize VWF in its activated form, which is, for instance, induced by immobilization, ristocetin, or VWD type 2B mutations. This unique feature allowed us to use this nanobody for the detection of activated VWF in solution. As a first example, the binding of recombinant wt VWF and recombinant VWF/R1306Q to immobilized nanobody AU/VWFa-11 was compared. Therefore, this particular nanobody was immobilized in microtiter wells and incubated with various concentrations (0-3.7 nM) of wt VWF and VWF/R1306Q in the absence and presence of ristocetin or botrocetin. The amount of bound VWF was subsequently monitored using HRP-conjugated polyclonal antibodies against VWF. With regard to wt VWF, some binding could be observed, but absorbance values remained below 0.3 (Figure 5A). The addition of ristocetin or botrocetin resulted in a strong increase in binding, represented by a 6-fold increase in absorbance (up to 1.85). We quantified this difference by calculating the respective slopes of the initial, linear parts of the curve. This revealed that the slope for VWF/ristocetin was increased 7.2-fold compared to wt VWF alone. A similar increase in slope compared to wt VWF could be observed for VWF/R1306Q in the absence of ristocetin (Figure 5A inset). Moreover, this increase was not further enhanced in the presence of ristocetin. Because activation of VWF with 1 mg/mL ristocetin can induce nonspecific interactions, such as flocculation of VWF, wt VWF was incubated with various concentrations of ristocetin. This revealed that maximal binding to AU/VWFa-11 was already reached at low ristocetin concentrations (250 μg/mL; Figure 5B). Taken together, this assay provides a useful tool to detect circulating VWF containing an A1 domain in active conformation.

Detection of activated VWF in patient plasma

Because nanobody AU/VWFa-11 was particularly efficient in the detection of active VWF in solution, we tested whether this nanobody could be used for the detection of active VWF in plasma from patients. First, we analyzed the plasma from patients previously defined as type 2B, as well as a group of healthy individuals. As a reference, NPP was used (see "Patients, materials, and methods"). The absorbance values obtained for NPP remained low

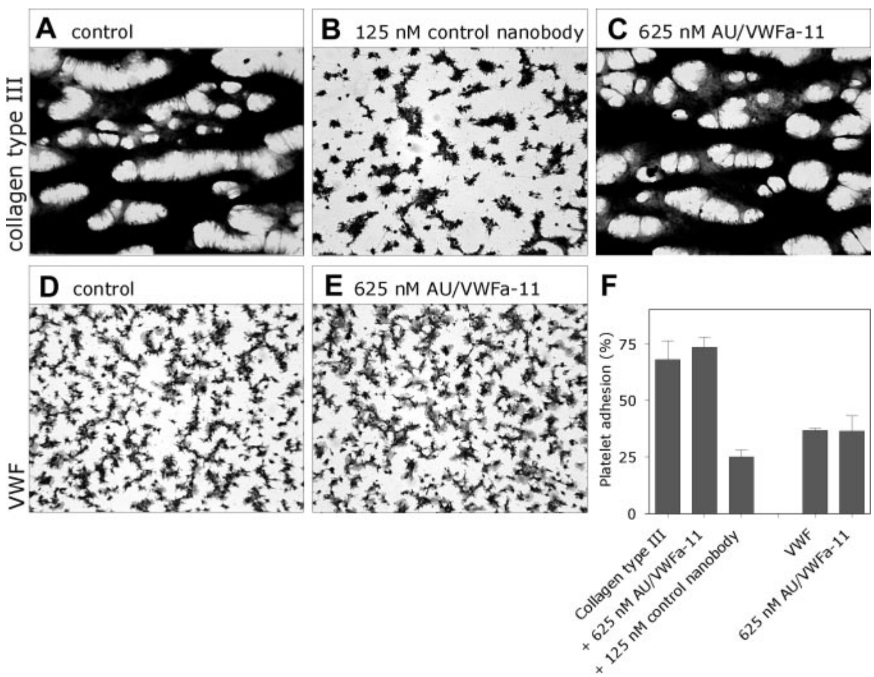

Figure 4. Different binding sites for GpIbα and AU/VWFa-11. (A-C) Whole blood was perfused over coverslips coated with collagen type III (30 μg/cm^2 in 0.05 M/L acetic acid) in the absence (A) or presence (B) of the control nanobody (125 nM) or AU/VWFa-11 (625 nM, C) at a shear rate of 1600 s^{-1} (D-E) Reconstituted blood was perfused over coverslips coated with pd VWF (15 μg/mL) in the absence (D) or presence of 625 nM AU/VWFa-11 (E) at a shear rate of 1600 s^{-1}. After perfusion, adhered platelets were fixed in 0.5% glutaraldehyde in PBS, dehydrated in methanol, and stained with May-Grünwald-Giemsa. Platelet aggregates are represented by the dark regions. (F) Platelet adhesion was evaluated using computer-assisted analysis and was expressed as the percentage of surface covered with platelets (n = 3). Adhered platelets were visualized using light microscopy (Leitz Diaplan; Leica, Rijswijk, the Netherlands) and computer-assisted analysis (AMS 40-10; Saffron, Walden, United Kingdom). Original magnification was 400 × (40 ×/1.00 NA objective lens).

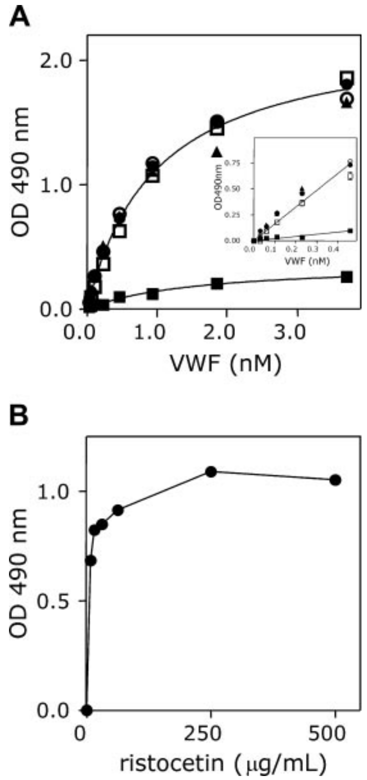

Figure 5. Effect of ristocetin, botrocetin, and the R1306Q mutation on binding to AU/VWFa-11. (A) Microtiter wells were coated overnight at 37°C with AU/VWFa-11 (5 μg/mL in 50 mM $NaHCO_3$, pH 9.6) and blocked 30 minutes at 37°C with 3% BSA, 0.1% Tween-20 in PBS. After washing, microtiter wells were incubated with medium containing different concentrations of wt VWF (squares, triangles) or VWF/R1306Q (circles; 0-3.7 nM). Binding was allowed for 1 hour at 37°C in the absence of modulators (■, ●), or in the presence of 1 mg/mL ristocetin (□, ●) or 0.2 U/mL botrocetin (▲). Microtiter wells were washed using 0.1% Tween-20 in PBS and incubated with HRP-conjugated polyclonal anti-VWF antibody. Bound VWF was detected by measuring peroxidase activity. An enlargement of the linear part of the binding curves is provided in the inset. Data represent the mean ± SD of 3 experiments. (B) AU/VWFa-11–coated microtiter wells were incubated with wt VWF in the presence or absence of various concentrations of ristocetin (0.08-1 mg/mL). After washing, wells were incubated with an HRP-conjugated polyclonal anti-VWF antibody. Bound VWF was detected by measuring the peroxidase activity.

(Figure 6A), and the slope was set to be 1. Also for each of the healthy individuals, only low absorbance values were detected, suggesting low amounts of active VWF in their plasma. A typical example of the slopes found for VWF type 2B patients is presented in Figure 6A. The mean slope compared to NPP was 0.70 ± 0.13 (n = 9; Figure 6B). In contrast, high amounts of active VWF could be determined in the plasmas of the VWD type 2B patients, as illustrated by the strongly increased absorbance values (Figure 6A). The mean slope was calculated to be 8.4 ± 4.5 (n = 10), a 12-fold increase compared to healthy individuals (P = .001; Figure 6B). Thus, this assay indeed seems to be useful to analyze the presence of active VWF in plasma of patients.

Correlation between VWF activation and platelet count

Interestingly, the activation factor determined for VWF in plasma from patients with VWD type 2B varied considerably (1.95-14.0). This variation was not found in plasma from healthy individuals (0.57-0.83). VWF containing type 2B mutations binds spontaneously to platelets, leading to enhanced clearance of both platelets and VWF. We therefore considered the possibility that the relative activation of VWF in circulation influenced the formation of platelet-VWF complexes. To address this question, we plotted the platelet counts obtained from the blood taken to prepare the plasma samples versus the corresponding activation factor of these plasmas. A strong inverse correlation was found between these parameters (Figure 6C; $P < .003$, $R^2 = 0.7401$).

Detection of active VWF in plasma from patients with TTP

A second group of patients analyzed for the presence of active VWF in their plasma were patients lacking ADAMTS13 activity, which was clinically manifested as TTP. Two groups could be distinguished: one group was defined as patients having a congenital deficiency of ADAMTS13 (n = 5), whereas a second group had an acquired deficiency of ADAMTS13 (n = 12). Compared to the

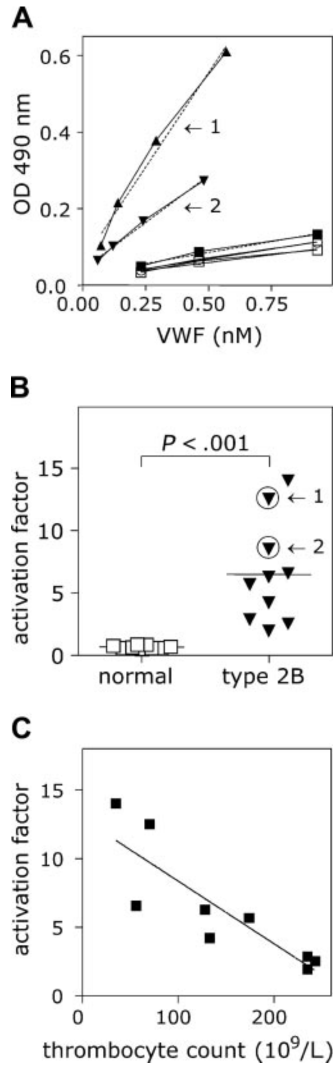

Figure 6. Activated VWF present in VWD type 2B plasma. (A) Microtiter wells coated with AU/VWFa-11 (5 μg/mL) were blocked 30 minutes with 3% BSA, 0.1% Tween-20 in PBS. NPP (■), plasma from healthy individuals (n = 9; □) and VWD type 2B plasma (n = 12; ▲, ▼) were diluted in PBS to obtain a concentration range (0.23-0.93 nM). After washing, wells were incubated 1 hour at 37°C with the diluted plasmas. Bound VWF was detected using HRP-conjugated polyclonal anti-VWF antibody. The concentration of VWF in the diluted samples was plotted against the measured OD 490 nm. The slope found for NPP was set to be 1. Arrows indicate the slopes found for 2 different VWD type 2B patients. (B) The activation factors were calculated and plotted in a scatter plot. Arrows indicate the activation factors calculated for patients 1 and 2 from panel A. The activation factor found for VWD type 2B patients was significantly higher than that for the healthy individuals ($P < .001$). Data represent the mean ± SD. (C) The activation factor calculated for 9 VWD type 2B patients was plotted against the thrombocyte counts in these samples and a correlation was found to be significant ($P < .003$; $R^2 = 0.7401$).

group of healthy individuals (see "Detection of activated VWF in patient plasma"), patients having acquired ADAMTS13 deficiency appeared to have increased levels of active VWF in their plasma (Figure 7A). The mean slope was calculated to be 1.52 ± 0.40, which is 2-fold higher compared to the group of healthy individuals ($P < .001$; Figure 7B). Also the patients with congenital ADAMTS13 deficiency contained active VWF in their plasma (Figure 7C). Interestingly, the amount of active VWF (slope $= 5.85 \pm 3.3$) was increased 8-fold compared to the healthy individuals ($P < .03$), but also 4-fold compared to the acquired ADAMTS13-deficient patients ($P < .05$; Figure 7D). Moreover, no overlap in slope values was observed between each of the healthy individuals and the 2 patient groups. This suggests that the assay may be useful for the diagnosis of ADAMTS13 deficiency in that it allows rapid distinction between acquired and congenital TTP.

Discussion

During the adhesion of platelets to the injured vessel wall, VWF functions as a molecular bridge between the exposed subendothelial matrix and the GpIb/IX/V complex. For the interaction between GpIbα and the A1 domain of VWF, the latter requires a conversion from its resting state into a GpIbα-binding conformation. Under several pathologic conditions, such as VWD type 2B and TTP, VWF is forced into its GpIbα-binding conformation leading to undesired, spontaneous interactions between VWF and platelets, a process that is often manifested via thrombocytopenia. Here, we describe a recombinant llama-derived antibody fragment that is able to distinguish between the resting and GpIbα-binding state of VWF. In addition, we show that this nanobody can be applied in the detection of such activated VWF in the plasma of different patient groups.

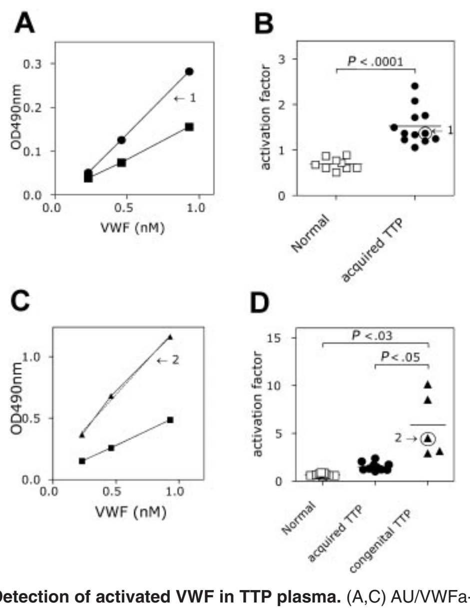

Figure 7. Detection of activated VWF in TTP plasma. (A,C) AU/VWFa-11–coated microtiter wells were incubated with NPP (■), plasma from healthy individuals ($n = 9$; □), and plasma from patients suffering from acquired TTP (A; $n = 12$; ■) or congenital TTP (C, $n = 5$, ▲). Plasma was diluted before incubation to obtain a concentration range of VWF (0.23-0.93 nM). Bound VWF was monitored with HRP-conjugated anti-VWF antibody. The amount of VWF in the diluted sample was plotted against the HRP activity (OD 490 nm). Slopes were calculated and the slope found for NPP was set to be 1. Arrows indicate the slopes found for a patient suffering from acquired TTP (1) or congenital TTP (2). (B-D) The activation factor was calculated and plotted in a scatter plot. Arrows indicate the values found for the patients plotted in panels A and C. Activation factors found for acquired and congenital TTP were significantly higher than those for the healthy individuals (acquired TTP versus healthy, $P < .001$ and congenital TTP versus healthy $P < .03$). The activation factor found for congenital TTP was also significantly elevated when compared to acquired TTP ($P < .05$). Data represent the mean ± SD.

Fuctional properties of nanobody AU/VWFa-11

Llamas produce a substantial part of their functional immunoglobulins as homodimers of heavy chains, so-called nanobodies. By using a phage-display approach, we have been able to isolate a nanobody (ie, AU/VWFa-11) that recognizes VWF in its GpIbα-binding conformation but not VWF in its soluble, resting state (Figure 1). Because our selection strategy included the isolated A1 domain of VWF, it is obvious that this nanobody is directed against this region of the molecule. Interestingly, AU/VWFa-11 displayed distinct interactions with the various recombinant A1 domain variants (Figure 2). First, the A1 domain variant with short flanking regions (VWF/A1(1261-1468)) was more efficient in binding to this nanobody compared to its counterpart with longer flanking regions (VWF/A1(1238-1481)). This suggests that the N- and C-terminal regions of the A1 domain may play a role in the exposure of the binding site for AU/VWFa-11. It is of interest to mention that these flanking regions also modulate the interaction between VWF and GpIbα.[33] Binding of VWF/A1(1261-1468) to AU/VWFa-11 was even more increased on the introduction of a type 2B mutation (R1306Q). This mutation also induces spontaneous binding between VWF and GpIbα.[24] Comparison of the various crystal structures revealed that the R1306Q replacement results in a number of conformation changes within the A1 domain, which may be responsible for improved GpIbα binding.[34] It seems conceivable that these changes also promote binding of nanobody AU/VWFa-11. In view of the similarities between this nanobody and GpIbα in their interaction with VWF, one would expect that both proteins share a similar binding site. Surprisingly, GpIbα and AU/VWFa-11 can interact simultaneously with VWF (Figure 3A). Moreover, nanobody AU/VWFa-11 is unable to interfere with the interaction between VWF and GpIbα (Figures 3B and 4). Thus, this nanobody and GpIbα seem to recognize different regions within the A1 domain, suggesting that changes in conformation on activation of the A1 domain are not limited to the GpIbα-binding site. At present, studies are in progress to define the epitope of AU/VWFa-11 in more detail.

Application of AU/VWFa-11 in the detection of active VWF in plasma from patients

Measurement of active VWF in plasma is currently assessed in an indirect manner by monitoring platelet aggregation in the presence of various concentrations of ristocetin. The unique properties of our nanobody allow the direct detection of active VWF in plasma, even under conditions of low antigen levels of VWF. This makes the immunosorbent assay suitable to analyze the presence of active VWF in the plasma of patients with pathologic conditions associated with reduced platelet numbers. In an initial attempt, we applied our assay to compare the presence of active VWF in healthy individuals and patients diagnosed as having VWF type 2B or TTP. Plasma of healthy individuals showed only little binding of VWF to immobilized AU/VWFa-11 (Figure 6), confirming that the majority of the circulating VWF is in a nonbinding conformation. Some residual binding was found, indicating that even under physiologic conditions a minor proportion of the VWF molecules could circulate in an activated conformation. Alternatively, some activation might have been introduced as a result of blood sampling and plasma preparation. An interesting issue in this regard is whether or not the introduction of the conformation changes is a reversible phenomenon. Unfortunately, our data do not distinguish between these possibilities, and further studies are therefore required.

Compared to the plasma from healthy individuals, increased amounts of active VWF were present in the plasma from patients with VWD type 2B or TTP (Figures 6-7). Although phenotypically distinct, both diseases are characterized by thrombocytopenia, caused by spontaneous platelet-VWF interaction. Indeed, an inverse correlation was found between the level of activated VWF in plasma from patients with VWD type 2B and their platelet count (Figure 6C). This may point to a direct role for activated VWF in the onset of thrombocytopenia.

Interestingly, when we incubated AU/VWFa-11 with plasma from patients with congenital TTP, we found that the amount of activated VWF was not only significantly elevated compared to healthy individuals, but also compared to patients with acquired TTP. Plasma samples of patients with acquired TTP were collected on admission to the hospital, before treatment with plasma exchange. At this time, a substantial part of the activated VWF is most likely present in the platelet-rich thrombi found in the microvasculature. This could explain the differences in levels of activated VWF between acquired and congenital TTP. On the other hand, the different molecular background of acquired and congenital TTP could also account for the difference in activation of VWF. Although further studies must be performed, the AU/VWFa-11 immunosorbent assay seems to have the potential to distinguish between acquired and congenital TTP.

In summary, we introduce a novel antibody fragment that is able to discriminate between the resting and activated state of VWF, and application of this nanobody enables us to detect activated VWF in plasma. As a consequence, this assay may be of particular interest for investigating the contribution of VWF to the pathogenesis of various vascular diseases that are characterized by thrombocytopenia.

Acknowledgments

We thank Dr J. A. Lopez for the GpIb-expressing CHO cells; Dr J. P. Girma for helpful comments; and K. De Smet, B. Van der Jeugt, M. J. Ijsseldijk, and Dr S. Tsuji for excellent technical contributions.

Consistent with *Blood* policy, nanobody AU/VWFa-11 is available to other investigators in the field. Requests should be addressed to the corresponding author (Dr P. J. Lenting).

References

1. Ruggeri ZM. Von Willebrand factor. Curr Opin Hematol. 2003;10:142-149.
2. Savage B, Saldivar E, Ruggeri ZM. Initiation of platelet adhesion by arrest onto fibrinogen or translocation on von Willebrand factor. Cell. 1996; 84:289-297.
3. Vicente V, Houghten RA, Ruggeri ZM. Identification of a site in the alpha chain of platelet glycoprotein Ib that participates in von Willebrand factor binding. J Biol Chem. 1990;265:274-280.
4. Huizinga EG, Tsuji S, Romijn RA, et al. Structures of glycoprotein Ibalpha and its complex with von Willebrand factor A1 domain. Science. 2002;297: 1176-1179.
5. Berndt MC, Du XP, Booth WJ. Ristocetin-dependent reconstitution of binding of von Willebrand factor to purified human platelet membrane glycoprotein Ib-IX complex. Biochemistry. 1988;27:633-640.
6. Scott JP, Montgomery RR, Retzinger GS. Dimeric ristocetin flocculates proteins, binds to platelets, and mediates von Willebrand factor-dependent agglutination of platelets. J Biol Chem. 1991;266: 8149-8155.
7. Ruggeri ZM. Von Willebrand factor, platelets and endothelial cell interactions. J Thromb Haemost. 2003;1:1335-1342.
8. Ruggeri ZM, Pareti FI, Mannucci PM, Ciavarella N, Zimmerman TS. Heightened interaction between platelets and factor VIII/von Willebrand factor in a new subtype of von Willebrand's disease. N Engl J Med. 1980;302:1047-1051.
9. Ruggeri ZM, Zimmerman TS. von Willebrand factor and von Willebrand disease. Blood. 1987;70: 895-904.
10. Ruggeri ZM, Ware J. The structure and function of von Willebrand factor. Thromb Haemost. 1992; 67:594-599.
11. Sadler JE. Biochemistry and genetics of von Willebrand factor. Annu Rev Biochem. 1998;67:395-424.
12. Wagner DD, Marder VJ. Biosynthesis of von Willebrand protein by human endothelial cells. Identification of a large precursor polypeptide chain. J Biol Chem. 1983;258:2065-2067.
13. Arya M, Anvari B, Romo GM, et al. Ultralarge multimers of von Willebrand factor form spontaneous high-strength bonds with the platelet glycoprotein Ib-IX complex: studies using optical tweezers. Blood. 2002;99:3971-3977.
14. Dong JF, Moake JL, Nolasco L, et al. ADAMTS-13 rapidly cleaves newly secreted ultralarge von Willebrand factor multimers on the endothelial surface under flowing conditions. Blood. 2002;100:4033-4039.
15. Fujikawa K, Suzuki H, McMullen B, Chung D. Purification of human von Willebrand factor-cleaving protease and its identification as a new member of the metalloproteinase family. Blood. 2001;98:1662-1666.
16. Gerritsen HE, Robles R, Lammle B, Furlan M. Partial amino acid sequence of purified von Willebrand factor-cleaving protease. Blood. 2001;98:1654-1661.
17. Moake JL. Thrombotic microangiopathies. N Engl J Med. 2002;347:589-600.
18. Levy GG, Nichols WC, Lian EC, et al. Mutations in a member of the ADAMTS gene family cause thrombotic thrombocytopenic purpura. Nature. 2001;413:488-494.
19. Remuzzi G, Galbusera M, Noris M, et al. von Willebrand factor cleaving protease (ADAMTS13) is deficient in recurrent and familial thrombotic thrombocytopenic purpura and hemolytic uremic syndrome. Blood. 2002;100:778-785.
20. Moake JL, Turner NA, Stathopoulos NA, Nolasco LH, Hellums JD. Involvement of large plasma von Willebrand factor (vWF) multimers and unusually large vWF forms derived from endothelial cells in shear stress-induced platelet aggregation. J Clin Invest. 1986;78:1456-1461.
21. George JN. How I treat patients with thrombotic thrombocytopenic purpura-hemolytic uremic syndrome. Blood. 2000;96:1223-1229.
22. Sodetz JM, Pizzo SV, McKee PA. Relationship of sialic acid to function and in vivo survival of human factor VIII/von Willebrand factor protein. J Biol Chem. 1977;252:5538-5546.
23. Lankhof H, van Hoeij M, Schiphorst ME, et al. A3 domain is essential for interaction of von Willebrand factor with collagen type III. Thromb Haemost. 1996;75:950-958.
24. Lankhof H, Damas C, Schiphorst ME, et al. Functional studies on platelet adhesion with recombinant von Willebrand factor type 2B mutants R543Q and R543W under conditions of flow. Blood. 1997;89:2766-2772.
25. Lenting PJ, Westein E, Terraube V, et al. An experimental model to study the in vivo survival of von Willebrand factor. Basic aspects and application to the R1205H mutation. J Biol Chem. 2004; 279:12102-12109.
26. Romijn RA, Westein E, Bouma B, et al. Mapping the collagen-binding site in the von Willebrand factor-A3 domain. J Biol Chem. 2003;278:15035-15039.
27. Arbabi GM, Desmyter A, Wyns L, Hamers R, Muyldermans S. Selection and identification of single domain antibody fragments from camel heavy-chain antibodies. FEBS Lett. 1997;414:521-526.
28. Skerra A, Pluckthun A. Assembly of a functional immunoglobulin Fv fragment in *Escherichia coli*. Science. 1988;240:1038-1041.
29. Lopez JA, Leung B, Reynolds CC, Li CQ, Fox JE. Efficient plasma membrane expression of a functional platelet glycoprotein Ib-IX complex requires the presence of its three subunits. J Biol Chem. 1992;267:12851-12859.
30. Lisman T, Moschatsis S, Adelmeijer J, Nieuwenhuis HK, de Groot PG. Recombinant factor VIIa enhances deposition of platelets with congenital or acquired alpha IIb beta 3 deficiency to endothelial cell matrix and collagen under conditions of flow via tissue factor-independent thrombin generation. Blood. 2003;101:1864-1870.
31. Veyradier A, Lavergne JM, Ribba AS, et al. Ten candidate ADAMTS13 mutations in six French families with congenital thrombotic thrombocytopenic purpura (Upshaw-Schulman syndrome). J Thromb Haemost. 2004;2:424-429.
32. Wu YP, Vink T, Schiphorst M, et al. Platelet thrombus formation on collagen at high shear rates is mediated by von Willebrand factor-glycoprotein Ib interaction and inhibited by von Willebrand factor-glycoprotein IIb/IIIa interaction. Arterioscler Thromb Vasc Biol. 2000;20:1661-1667.
33. Nakayama T, Matsushita T, Dong Z, et al. Identification of the regulatory elements of the human von Willebrand factor for binding to platelet GPIb. Importance of structural integrity of the regions flanked by the CYS1272-CYS1458 disulfide bond. J Biol Chem. 2002;277:22063-22072.
34. Dumas JJ, Kumar R, McDonagh T, et al. Crystal structure of the wild-type von Willebrand factor A1-glycoprotein Ibalpha complex reveals conformation differences with a complex bearing von Willebrand disease mutations. J Biol Chem. 2004;279:23327-23334.